Registration of Hyperpolarized Helium-3 Diffusion MR Images for the Assessment of Changes with Albuterol Treatment in COPD Patients

PD Burstein[1], JP Mugler III[2], EE de Lange[2], J Mata[2], K Ruppert[2], TA Altes[2]

[1]School of Biomedical Engineering, Science and Health Systems, Drexel University, 3141 Chestnut St., Philadelphia, PA 19111

[2]Department of Radiology University of Virginia, Box 800170, Charlottesville, VA 22908

pablo.d.burstein@drexel.edu, taa2c@virginia.edu

Abstract

Our preliminary results show that albuterol administered to patients with chronic obstructive pulmonary disease (COPD) has no significant effect on the local ADC (apparent diffusion coefficient) values. To prevent confounds stemming from airway dilatation to affect albuterol's effect on COPD, we compute ADC and ADC difference maps over ventilated regions only. We compare intra-subject ADC values of pre and post albuterol administration conditions through the computation of RMSE, a voxel-wise based metric, in order to avoid compensation likely to occur in the computation of the (global) mean-ADC difference. Voxel-wise comparison is achieved through coregistration and normalization of the b0 images previously masked with corresponding combined ventilation masks (zero in unventilated voxels), both in the pre and the post albuterol reference spaces. The ADC and ADC difference maps are also computed for ventilated-only voxels. We also show that the registration process does not affect global ADC metrics.

Introduction

Hyperpolarized helium-3 is a gaseous contrast agent for MR imaging that, when inhaled, provides high temporal and spatial resolution images of the airspaces of the lung (1, 2). By measuring the spin density of the inhaled helium, images of lung ventilation can be obtained (3). Focal areas of poor ventilation have been demonstrated in a variety of lung diseases including asthma (4), chronic obstructive pulmonary disease (COPD) (2, 5), and cystic fibrosis (6, 7). In addition to ventilation imaging, the size and connectedness of the alveoli/distal airspaces can be assessed using diffusion techniques, similar to those used in brain MRI (8, 9). Elevated apparent diffusion coefficients (ADC) have been found in patients with COPD (10) and in animal models of emphysema (11, 12). These elevated ADC values are thought to correspond to the distal airspace enlargement that characterizes emphysema (12). To date, analysis of hyperpolarized helium-3 ADC maps has largely been confined to histogram based approaches, adequate for studies in which each subject is imaged a single time to assess for disease presence/severity, but that do not

take advantage of spatial or regional information contained within the ADC maps (8, 11, 13, 14). In order to assess changes on a regional basis, more sophisticated image analysis methods are required if the subjects are imaged more than once. One potential difficulty in developing a method to assess regional changes in the ADC maps is that the pattern of ventilation in the lung may vary with time or treatment (15). Since the ADC can only be measured in ventilated regions of the lung, comparison of ADC values at different time points is only meaningful at sites where the voxels are ventilated at the examined time-points.

The purpose of this study is to assess the effect of albuterol on COPD (emphysema) patients through the local analysis of the corresponding ADC maps. Our approach intends to circumvent the problem arising from the use of global metrics, such as difference of means, requiring no alignment of the pre and post-albuterol administration images, but suffering from possible compensation due to complementary changes, potentially leading to misinterpretation of the results (e.g.., false negative). In the following, we describe a newly developed paradigm for the computation of always-ventilated ADC difference maps. Our approach allows for the computation of locally based metrics such as RMSE. We present preliminary results when this algorithm is applied to a small group including healthy (normal) subjects and COPD patients.

Methods

Acquisition Protocol

Hyperpolarized helium diffusion MR imaging was performed in 6 subjects (2 healthy and 4 with COPD) with each subject being imaged before and after the administration of inhaled albuterol on two successive days (Day1, and Day2). Thus, 4 ADC maps were obtained for each subject. Albuterol is a bronchodilator and as such could change the regional pattern of ventilation but is not expected to affect alveolar morphology, i.e, ADC. All subjects underwent spirometry immediately prior to the helium MR scan on each of the two imaging days. The hyperpolarized helium gas was administered with approval from the Food and Drug Administration (FDA) as an Investigational New Drug (IND # 57,866), and this study was approved by our local institutional review board (IRB) with written informed consent was obtained from all subjects.

The helium-3 gas was polarized in a commercial helium polarizer (Model IGI9600 Helium Polarizer; Magnetic Imaging Technologies Inc., Durham, NC) by the collisional spin-exchange method and polarizations of 30 to 40% were typically achieved. Approximately 300 mL of polarized helium-3 gas was mixed with approximately 700 mL of medical grade nitrogen and dispensed into a Tedlar bag (Jensen Inert Products, Coral Springs, FL). The bag containing the helium dose was then taken to the MR scanner room where the subject was already positioned supine within the 1.5 T whole body MR scanner (Magnetom Sonata, Siemens Medical Solutions, Malvern, PA) equipped with the multinuclear imaging option. A flexible wrap coil (IGC Medical Advances, Milwaukee, WI) tuned to the helium-3 frequency was used for imaging. Starting from maximum expiration, subjects inhaled the hyperpolarized helium/nitrogen mixture from the bag through a short segment of plastic tubing. During the subsequent breath hold, contiguous axial diffusion-weighted images that covered the whole lung volume were acquired by using a

FLASH-based pulse sequence (TR/TE, 11/6.7 ms; FA, 7°; matrix, 80 x 128; FOV, 37 x 42 cm, slice thickness, 20 mm). Diffusion sensitization was achieved by the addition of a bipolar gradient-pulse pair in the slice-select direction. Images were obtained corresponding to two b-values, 0, and 1.6 s/cm^2, namely b_0 and $b_{1.6}$. The images collected at b=0 s/cm^2 depict regional ventilation. To minimize the effects of signal attenuation from T1 decay and from radio-frequency pulses, the data corresponding to both b-values were acquired for a given phase-encoding view before the phase-encoding gradient strength was incremented to its next value. Assuming mono-exponential signal loss due to diffusion, two diffusion-weighted images, each corresponding to a different b value, are the minimum number required to calculate a spatial map of the ADC values. Since the goal was to image subjects with COPD whose breath hold capacity may be limited, we elected to use the minimum number of b-values to minimize the breath hold duration. The length of the breath hold depended on the number of images required to cover the entire lung volume but was typically less than 15 sec.

ADC Difference Map Computation

As opposed to anatomical images, such as those obtained from CT, hyperpolarized gas images of the lung tend to present substantial variation in the apparent anatomy at different acquisition times, depending on different temporal functional characteristics, such as ventilation and diffusion. In our case, this varying apparent anatomy may also arise as the result of different areas of the lung being ventilated before and after drug administration, and give place to local functional pattern differences, which may erroneously drive the registration. Since our focus is albuterol effect on COPD, i.e., the ADC maps within emphysematous tissue, we want to disregard ventilation changes at the airways level. To this end, our first step is to compute ventilated-only versions of the measured images (and, as a consequence, of the corresponding ADC maps), which will then be used during this study. This also ensures that the registration of the pre and post-albuterol images is driven by ventilated voxels only, thus preventing erroneous deformation into unventilated areas (likely to occur to match anatomy). For the sake of simplicity, we will use *pre* and *post* for short for *pre-albuterol* and *post-albuterol* administration, respectively.

For each subject, we first compute M_{Vpre} and M_{Vpost}, the pre and post ventilation binary masks, corresponding to b_{0pre} and b_{0post}, the pre and post b_0 (b = 0 s/cm^2) images, respectively. These masks, encoding ventilation pre and post-albuterol, are obtained by thresholding b_{0pre} and b_{0post} using Otsu's algorithm (17) (given our acquisition system, we assume SNR>2 for approximate Gaussian distribution). Then, in order to obtain combined ventilation masks both in pre (M_{CVpre}) and post (M_{CVpost}) reference spaces, we coregister b_{0post} into b_{0pre}, and apply the obtained transformation to M_{Vpost} to obtain M_{Vpost_inpre}. In turn, we apply the inverse transformation to M_{Vpre} to obtain M_{Vpre_inpost}. Since this study deals with intra-patient comparisons, where the acquisition was carefully performed to replicate same conditions, we assume the combined ventilation masks, obtained through coregistration only, to be accurate enough to closely match the actual ventilated regions. Finally, the combined vetilation mask in the pre space, $M_{CVpre,}$ and its counterpart in the post space, M_{CVpost}, are obtained by:

$$M_{CVpre} = M_{Vpre} * M_{Vpost\_inpre} \quad (1)$$

$$M_{CVpost} = M_{Vpre\_inpost} * M_{Vpost} \quad (2)$$

where * stands for pixel-wise multiplication. M_{CVpre} and M_{CVpost} have a value of 1 wherever the lungs are *always* ventilated, and 0 otherwise. Next, the *always* ventilated versions of b_{0pre} and b_{0post}, namely b_{0Vpre} and b_{0Vpost}, respectively, are obtained by masking:

$$b_{0Vpre} = b_{0pre} * M_{CVpre} \quad (3)$$

$$b_{0Vpost} = b_{0post} * M_{CVpost} \quad (4)$$

Similarly, we compute $b_{1.6Vpre}$ and $b_{1.6Vpost}$ (b = 1.6 s/cm^2). Coregistration is implemented using a two-step multi-resolution paradigm, where a quaternion transform, used to take care of translation, and rotation, is followed by an affine transform, which "fine-tunes" for any possible (generally minor) shear and scaling.

Following, b_{0Vpre} and b_{0Vpost} are coregistered, using the same method described above, and normalized through a (deformable) symmetric diffeomorphic (topography preserving) algorithm (16). This last step is introduced to correct any deformation caused by imaging setup/inflation. Since our objective is to align voxels corresponding to the same anatomical location but possibly presenting different ADC values (as a consequence of the albuterol administration), a metric suitable for multi-modality registration is necessary. In our case, we use mutual information (MI) as the similarity metric both for the non-deformable and deformable steps, already proven to be very efficient in multi-modality registration, and very suitable for small deformations (18, 19, 20, 21, 22). Finally, we warp b_{0Vpost} and its corresponding $b_{1.6Vpost}$ into pre space, to match b_{0Vpre} and $b_{1.6Vpre}$, respectively. Pre and post ADC maps are then computed using the general equation:

$$ADC(x) = \frac{1}{1.6} \log \frac{b_0(x)}{b_{1.6}(x)} \quad (5)$$

where b_0(x) is the signal intensity of the voxel in b_0 and $b_{1.6}$(x) s the signal intensity of the corresponding voxel in $b_{1.6}$. We compute ADC using (1) for ventilated voxels only (Figure 1); unventilated voxels are set to zero in the ADC map. Notice the ventilation difference between pre and post-albuterol observed particularly in the upper right and upper left lobe in the b_0 images. Another advantage of using the combined ventilation masks is background noise removal, limiting the map to meaningful ADC values only, and, as a consequence, to more robust statistics.

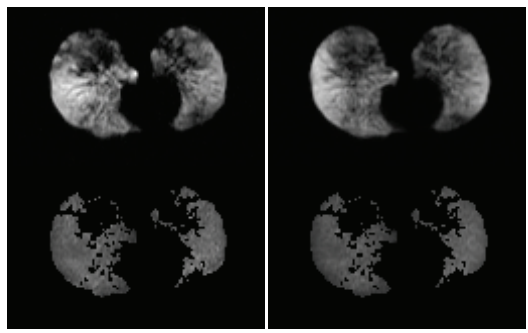

Figure 1. Pre (left) and post (right) albuterol b0 images (top) and corresponding ventilated ADC maps (bottom). ADC values are non-zero for ventilated voxels only. Ventilation differences between pre and post-albuterol is mainly observed in the upper right and upper left lobe in the b_0 images (top row).

Finally the ADC difference map, ΔADC, is computed as:

$$\Delta ADC = ADC_{post} - ADC_{pre} \qquad (6)$$

where ADC_{pre} and ADC_{post} are the values of ADC before and after albuterol administration. All our algorithms are implemented in C++ using The Insight Toolkit (ITK) libraries (18).

Validation

We compare global metrics commonly used in clinical assessment and tracking of COPD to assess whether warping affects the (warped) ADC map. These metrics, namely mean, rate of ADC above 0.35, 50% (median) and 90% percentile, are computed for the warped and non-warped (original) ADC post albuterol maps for each subject. As well, we establish basal acquisition variability, i.e., our control, by comparison of intra-subject images taken on Day1 and Day2 (Day1+1), without albuterol administration (pre).

Results

Warping Effect on ADC values

We are interested in assessing whether warping b_0 and $b_{1.6}$ images affects the corresponding ADC map computation in the new reference space. Table 1 shows the $\overline{ADC}$, % voxels with ADC ≥ 0.35, 50th (median) and, 90th percentiles for the post albuterol administration images, at Day1, before and after warping, along with the corresponding relative change (the last column). In general, it can be said that the global measures for the warped ADC map are not significantly different from the ones in the one computed in the acquisition (original) space. This is a desirable outcome if

one wants to compare ADC maps in a voxel-wise fashion. Relative high variation, though, is seen for the % voxels with ADC ≥ 0.35 measures, corresponding to subjects #1 and #3, with -53.19% and -66.62%, respectively. Despite these relative large changes, the absolute change is actually small, and can be explained as a consequence of interpolation limitations of the warped images; the negative change trend can be explained as interpolation towards background, given the general lack of signal in these images. Furthermore, the warped results still agree with the fact that these are normal subjects (low ADC signal).

#	$\overline{ADC}$ unwarped	$\overline{ADC}$ warped	%Δ
1	0.2362	0.2347	-0.63
2	0.3439	0.3367	-2.08
3	0.2286	0.2286	0.03
4	0.4625	0.4595	-0.66
5	0.3374	0.3347	-0.79
6	0.5272	0.5307	0.66

#	50th Percentile (median) unwarped	warped	%Δ
1	0.2331	0.2327	-0.17
2	0.3361	0.3332	-0.88
3	0.2247	0.2267	0.91
4	0.4554	0.4571	0.36
5	0.2960	0.2942	-0.61
6	0.5296	0.5338	0.80

#	% voxels with ADC ≥ 0.35 unwarped	warped	%Δ
1	1.56	0.73	-53.19
2	44.40	41.86	-5.72
3	1.65	0.55	-66.62
4	78.61	79.46	1.08
5	34.10	34.13	0.08
6	93.06	94.67	1.73

#	90th Percentile Unwarped	warped	%Δ
1	0.2863	0.2707	-5.45
2	0.4763	0.4456	-6.45
3	0.2870	0.2688	-6.34
4	0.6470	0.6266	-3.16
5	0.5155	0.5064	-1.76
6	0.6700	0.6598	-1.51

Table 1. Unwarped, warped, and percentage change for $\overline{ADC}$, % voxels with ADC ≥ 0.35, and 50th (median) and, 90th percentiles. Day1, post-albuterol. The warping process shows little effect on most of the metrics. *ADC* change seen is less than 0.8%, 0.92% for the median, and 1.77% for the 90th percentile. Relatively elevated change is seen for % voxels with ADC ≥ 0.35 for the normal subjects (53.19% for subject #1 and 66.62% for subject #3). Still, the corresponding values for these subjects are very low, still being negligible after such a change.

Basal Variability

Table 2 shows the basal variability expected at two acquisition times, Day1 and Day2 = Day1+1, without albuterol administration. In general, no significant change is seen from Day1 to Day2. This result suggests that basal variability is negligible.

#	$\overline{ADC}_{Day1}$	$\overline{ADC}_{Day2}$	RMSE
1	0.2334	0.2286	0.0380
2	0.3610	0.3473	0.0713
3	0.2144	0.2141	0.0461
4	0.4858	0.4603	0.1072
5	0.3115	0.3489	0.0995
6	0.5312	0.5390	0.0746

Table 2. Basal variability. Measurements taken at Day1 and Day2. No albuterol administered (pre images). RMSE show no significant change, suggesting negligible basal variability, and, therefore, suitability for treatment assesment and tracking.

Albuterol Effect

Table 3 and Figure 2 show the albuterol effect on the ADC maps. Table 3 presents similar values to those obtained for the basal variability, Table 2. This suggests, as it was expected, that albuterol has no significant effect neither on the normal subjects (#1 and #3) nor on the COPD patients. This result tends to confirm the hypothesis that, in the short term, albuterol does not change the emphysematous tissue characteristics with respect to the size of the voids created by the degeneration process.

#	$\overline{ADC}_{Pre}$	$\overline{ADC}_{Post}$	RMSE
1	0.2334	0.2362	0.0431
2	0.3610	0.3439	0.0709
3	0.2144	0.2286	0.0462
4	0.4858	0.4625	0.1001
5	0.3115	0.3374	0.0625
6	0.5312	0.5272	0.0798

Table 3. Albuterol effect. Measurements taken at Day1, pre and post albuterol administration. In general, RMSE show little change, suggesting that albuterol has no effect on subjects.

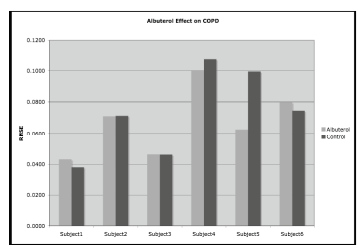

Figure 2. RMSE values for Albuterol administration effect are similar to those of the baseline (control) for all the subjects (subject #5 even shows higher degree of change for control than for albuterol administration). This suggests that there is no significant effect of albuterol.

Conclusions

We developed a method for voxel-wise comparison of hyperpolarized helium-3 ADC maps obtained in the same patient at different times. This method includes in the analysis only those regions of the lung that are ventilated at both time points (*always ventilated*) since the ADC cannot be measured in non-ventilated regions of the lung. This was achieved through the creation of combined ventilation masks in the pre and post-albuterol spaces. To test this algorithm, we imaged normal volunteers and patients with COPD before and after the administration of albuterol. As a bronchodilator, albuterol would be expected to change the pattern of ventilation but not the ADC values in ventilated regions of the lung. As expected, the patients with COPD present elevated ADC values as compared to the normal subjects, even after albuterol administration (while ventilation pattern changes were indeed observed in the patients). We found that the registration method, non-deformable followed by symmetric diffeomorphic algorithm with MI as the similarity metric, renders a good normalization of the pre and post-albuterol (as well as Day 1/Day2) images despite the ventilation changes while it does not significantly affect the global metrics. In addition, basal variability at acquisitions one day apart (Day 1/Day 2) was computed, providing the baseline for change detection. Finally, we found that there is little change in the ADC values before and after albuterol administration; i.e., RMSE of ADC difference maps support the hypothesis that no significant local change in ADC values, hence no significant change in the state of the emphysematous tissue, occurs as the result of albuterol administration.

References

1. Middleton H, Black RD, Saam B, et al. MR imaging with hyperpolarized 3He gas. Magn Reson Med 1995; 33:271-275.
2. Kauczor HU, Hofmann D, Kreitner KF, et al. Normal and abnormal pulmonary ventilation: visualization at hyperpolarized He-3 MR imaging. Radiology 1996; 201:564-568.
3. Altes TA, Rehm PK, Harrell F, Salerno M, Daniel TM, De Lange EE. Ventilation imaging of the lung: comparison of hyperpolarized helium-3 MR imaging with Xe-133 scintigraphy. Acad Radiol 2004; 11:729-734.
4. Altes TA, Powers PL, Knight-Scott J, et al. Hyperpolarized 3He MR lung ventilation imaging in asthmatics: preliminary findings. J Magn Reson Imaging 2001; 13:378-384.
5. de Lange EE, Mugler JP, 3rd, Brookeman JR, et al. Lung air spaces: MR imaging evaluation with hyperpolarized 3He gas. Radiology 1999; 210:851-857.
6. Donnelly LF, MacFall JR, McAdams HP, et al. Cystic fibrosis: combined hyperpolarized 3He-enhanced and conventional proton MR imaging in the lung--preliminary observations. Radiology 1999; 212:885-889.
7. Mentore K, Froh DK, de Lange EE, Brookeman JR, Paget-Brown AO, Altes TA. Hyperpolarized HHe 3 MRI of the lung in cystic fibrosis: assessment at baseline and after bronchodilator and airway clearance treatment. Acad Radiol 2005; 12:1423-1429.

8. Saam BT, Yablonskiy DA, Kodibagkar VD, et al. MR imaging of diffusion of (3)He gas in healthy and diseased lungs. Magn Reson Med 2000; 44:174-179.
9. Mugler JP, 3rd, Brookeman JR, Knight-Scott J, Maier T, de Lange EE, Bogorad PL. Regional measurement of the 3He diffusion coefficient in the human lung. In:In: Proceedings of the 6th Annual Meeting of ISMRM. Sydney, Australia, 1998; 1906.
10. Salerno M, Altes TA, Brookeman JR, de Lange EE, Mugler JP, 3rd. Rapid hyperpolarized 3He diffusion MRI of healthy and emphysematous human lungs using an optimized interleaved-spiral pulse sequence. J Magn Reson Imaging 2003; 17:581-588.
11. Chen XJ, Hedlund LW, Moller HE, Chawla MS, Maronpot RR, Johnson GA. Detection of emphysema in rat lungs by using magnetic resonance measurements of 3He diffusion. Proc Natl Acad Sci U S A 2000; 97:11478-11481.
12. Mata JF, Altes TA, Cai J, et al. Evaluation of emphysema severity and progression in a rabbit model: comparison of hyperpolarized 3He and 129Xe diffusion MRI with lung morphometry. J Appl Physiol 2007; 102:1273-1280.
13. Fain SB, Panth SR, Evans MD, Wentland AL, Holmes JH, Korosec FR, O'Brien MJ, Fountaine H, Grist TM. Early emphysematous changes in asymptomatic smokers: detection with 3He MR imaging. Radiology. 2006 Jun; 239(3):875-83.
14. Salerno M, de Lange EE, Altes TA, Truwit JD, Brookeman JR, Mugler JP, 3rd. Emphysema: hyperpolarized helium 3 diffusion MR imaging of the lungs compared with spirometric indexes--initial experience. Radiology 2002; 222:252-260.
15. Samee S, Altes T, Powers P, et al. Imaging the lungs in asthmatic patients by using hyperpolarized helium-3 magnetic resonance: assessment of response to methacholine and exercise challenge. J Allergy Clin Immunol 2003; 111:1205-1211.
16. Avants BB, Grossman M, Gee JC, Symmetric Diffeomorphic Image Registration: Evaluating Automated Labeling of Elderly and Neurodegenerative Cortex and Frontal Lobe. WBIR 2006: 50-57
17. Otsu, N. A thresholding selection method for grey-level histograms. IEEE Trans Systems, Man and Cybernetics SMC-9(1), 1979; 62-66.
18. Insight Toolkit. www.itk.org
19. Maes F, Collignon A, Vandermeulen D, Marchal G, and Suetens P. Multimodality Image Registration by Maximization of Mutual Information. IEEE Trans. Med. Imag., vol. 16, pp. 187–198, Apr. 1997.
20. Brown LG. A Survey of Image Registration Techniques. ACM Comput. Surv. vol. 24, pp. 325–376, 1992.
21. Viola P and Wells W. Alignment by Maximization of Mutual Information. Proc. 5th Int. Conf. Computer Vision, 1995, pp. 16–23
22. Karaçali B. Information Theoretic Deformable Registration Using Local Image Information. Int. Jour. of Computer Vision, vol. 72 issue 3